ADVANCED MATERIALS TECHNOLOGIES

Supporting Information

for *Adv. Mater. Technol.,* DOI: 10.1002/admt.202201472

4D Printing of Supramolecular Liquid Crystal Elastomer Actuators Fueled by Light

*Sean J. D. Lugger, Lorena Ceamanos, Dirk J. Mulder, Carlos Sánchez-Somolinos, and Albert P. H. J. Schenning**

Supporting Information

4D Printing of Supramolecular Liquid Crystal Elastomer Actuators Fueled by Light

*Sean J. D. Lugger, Lorena Ceamanos, Dirk J. Mulder, Carlos Sánchez-Somolinos, and Albert P. H. J. Schenning**

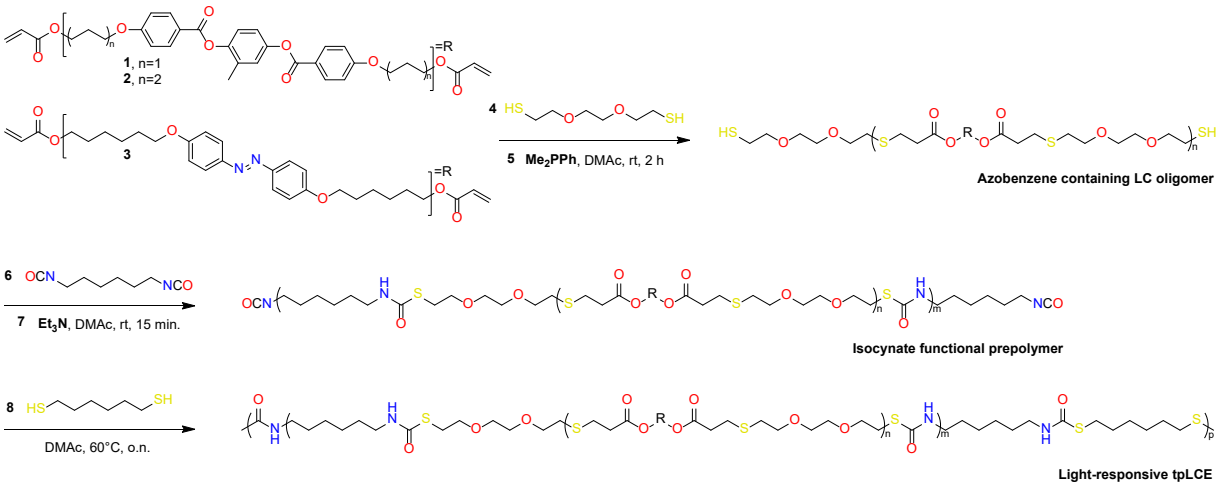

Figure S1. Synthesis of the light-responsive supramolecular, thermoplastic LCE (tpLCE)

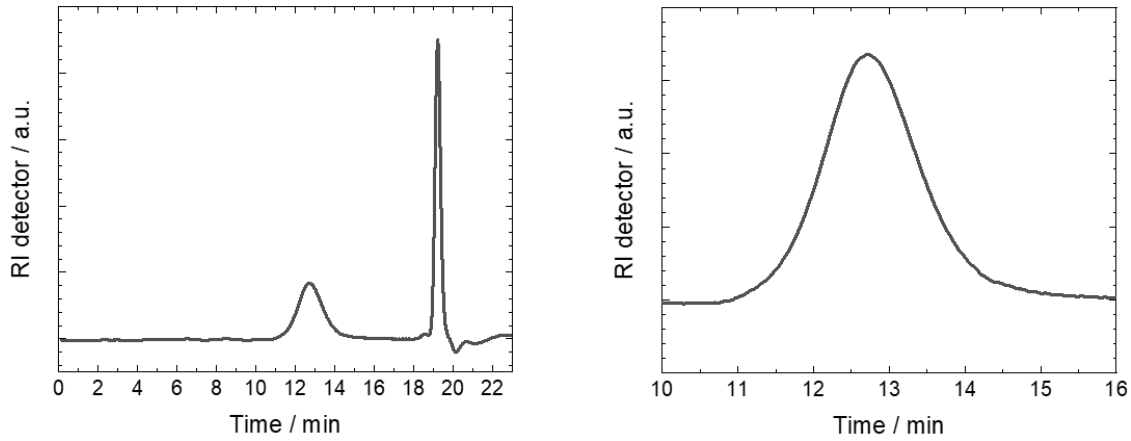

Figure S2. GPC data of the crude PTU (M_n = 77247 g mol^{-1} and polydispersity $Đ$ = 1.97) showing the full (left) and zoomed-in (right) chromatogram. The flow marker (toluene) is observed around 19 min.

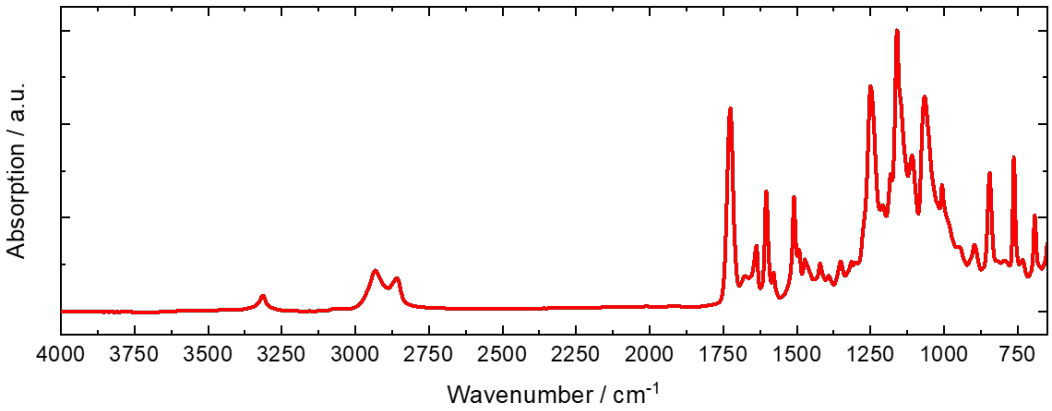

Figure S3. FT-IR spectrum of the crude PTU showing the absence of thiol ($\tilde{\nu} \approx 2560$ cm^{-1}) and isocyanate ($\tilde{\nu} \approx 2270$ cm^{-1}) stretching vibrations and the presence of TU amine ($\tilde{\nu} \approx 3310$–3340 cm^{-1}) and carbonyl stretching vibrations ($\tilde{\nu} \approx 1640$–1680 cm^{-1}).

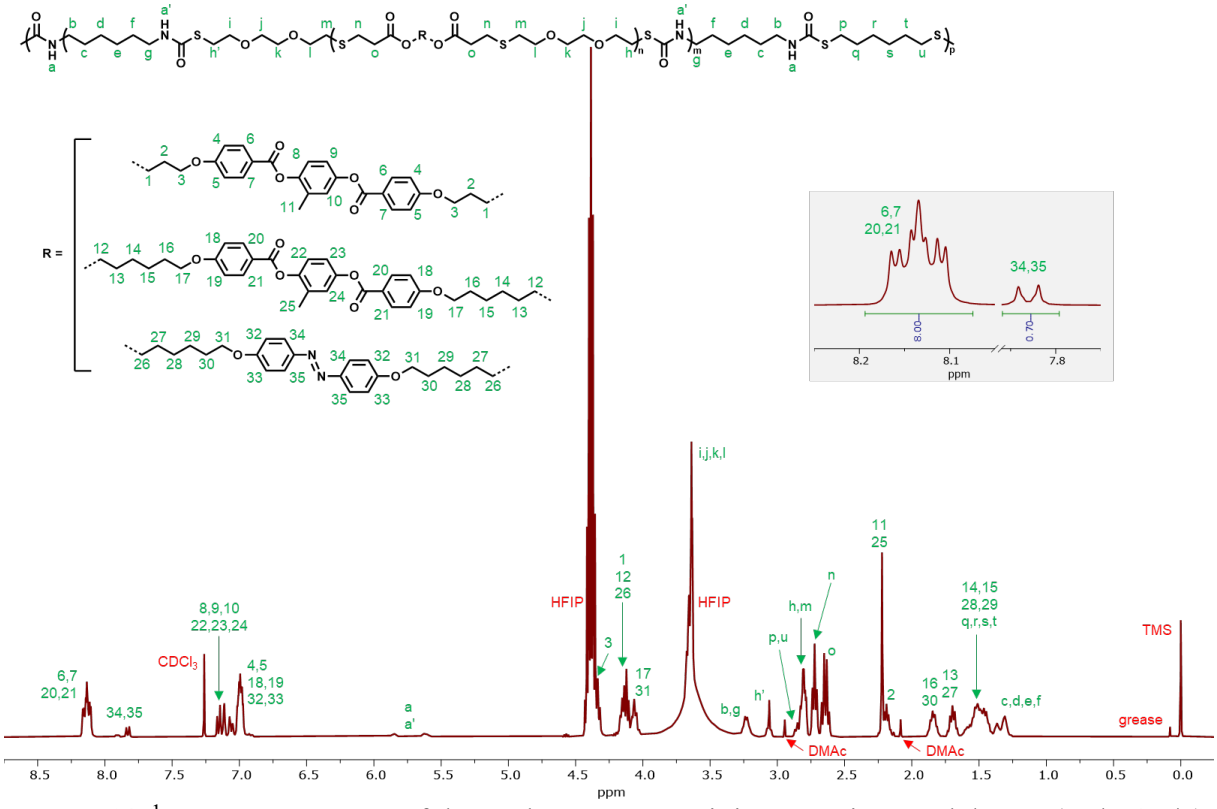

Figure S4. ^{1}H-NMR spectrum of the azobenzene containing PTU in $CDCl_3$/HFIP (95/5% v/v). The inset displays the aromatic protons of the mesogens (**1** and **2**) and azobenzene moiety (**3**). The integral around 8.13 ppm is set to 8.0 to match the number of protons of the benzene rings from the mesogens. Accordingly, based on this, the integral of the azobenzene around 7.83 ppm is determined to be 0.70. The ratio between these integrals is 0.09 (0.70 / 8.00), which corresponds perfectly to the used molar ratio of the azobenzene and LCs for the synthesis being 0.09 (2.64 mmol of **3** / (14.67 + 14.67 mmol **1** and **2**)).

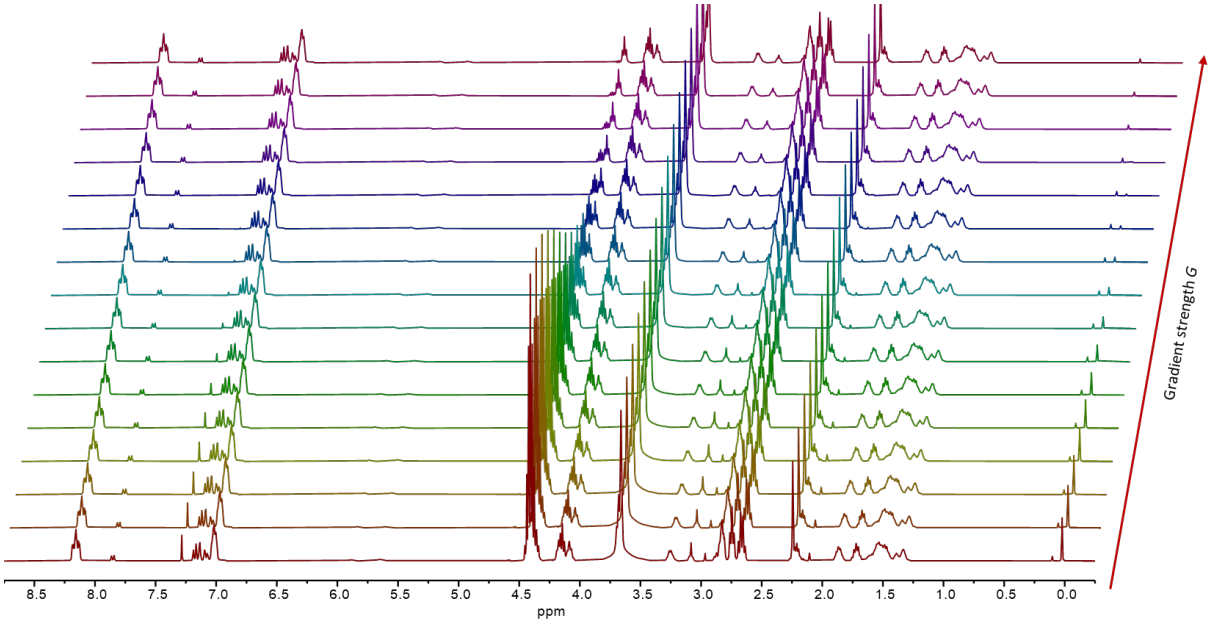

Figure S5. Stacked ^{1}H-NMR spectrum of the azobenzene containing PTU as a function of gradient strength *G* (pulse amplitude).

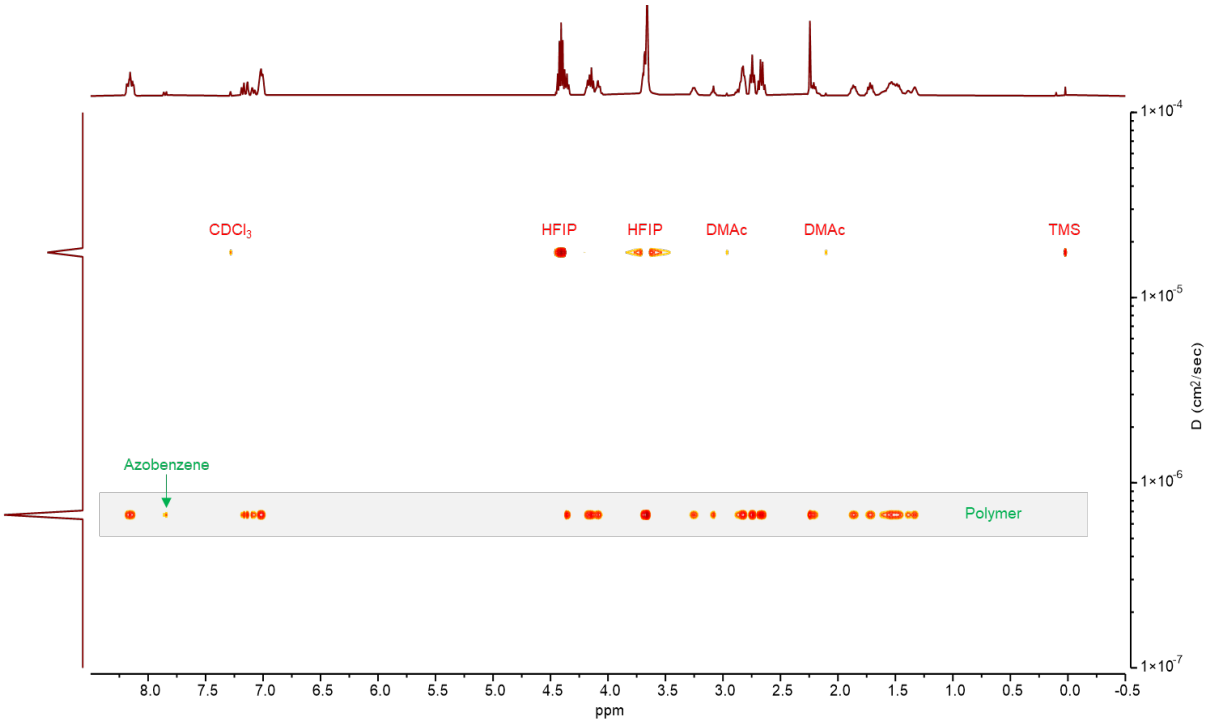

Figure S6. 2D DOSY spectrum of the azobenzene containing PTU showing two separate diffusion traces. The diffusion coefficients (*D*) of the azobenzene moiety and the polymer are the same, indicating the successful incorporation of the azobenzene into the PTU during synthesis. In contrast, the smaller solvent and tetramethylsilane (TMS) molecules exhibit a high diffusion coefficient.

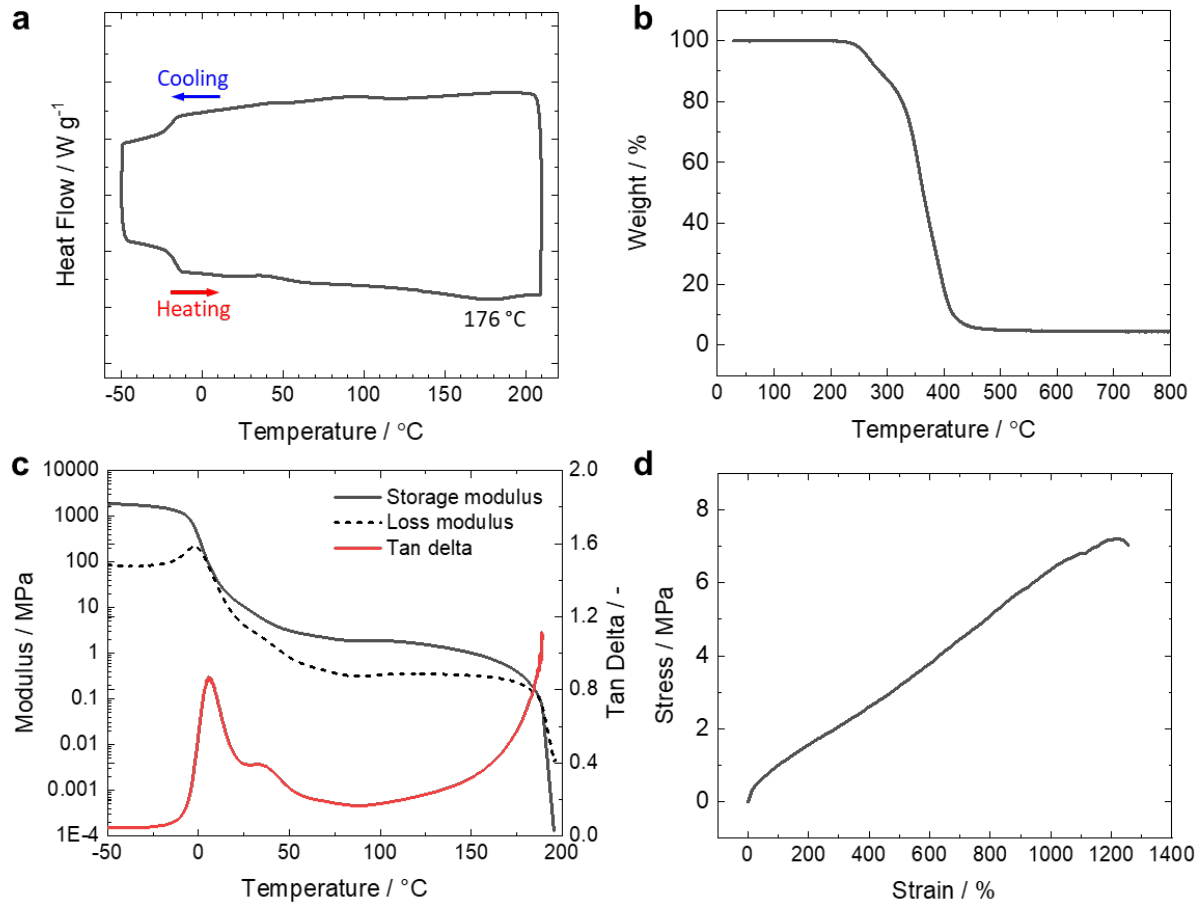

Figure S7. Thermal and mechanical characterization of the PTU. a) DSC thermograph of the second heating and cooling run. b) TGA profile. c) DMA storage modulus (*E*'), loss modulus (*E*"), and loss tangent. d) Stress-strain curves at room temperature.

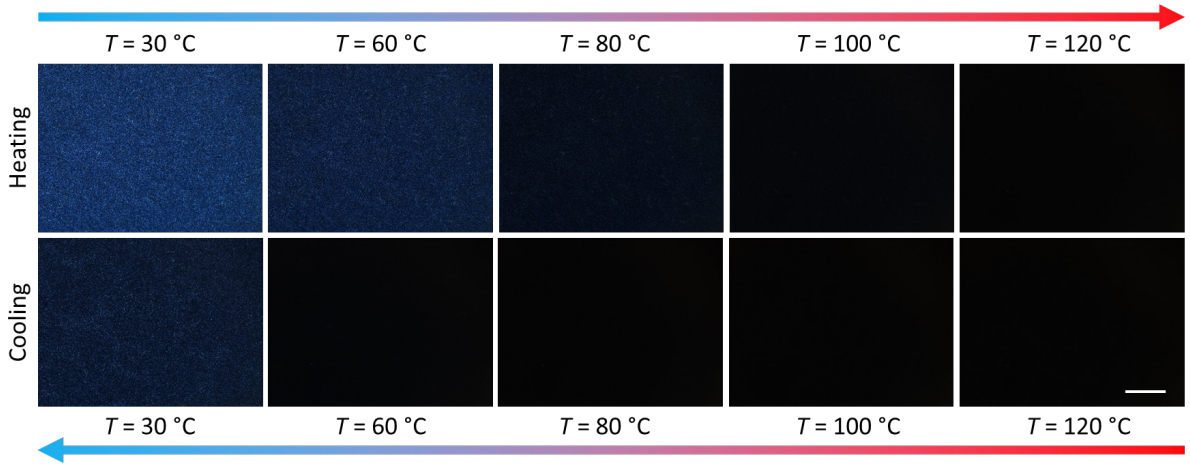

Figure S8. POM images of the PTU LCE showing the loss in birefringence upon heating, which slowly reappears with a large thermal hysteresis when cooled. The scale bar represents 200 µm.

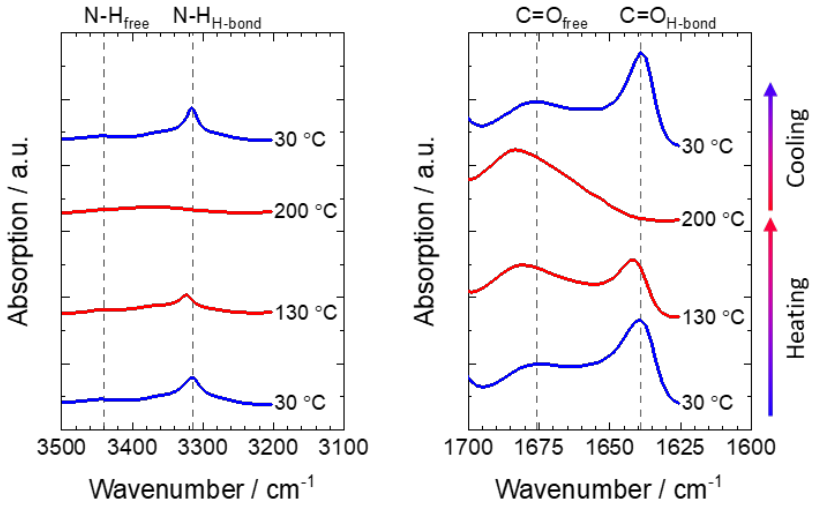

Figure S9. Temperature-dependent FT-IR spectra showing free and hydrogen-bonded thiourethane amine (left) and carbonyl (right) stretching vibrations. Upon heating, the hydrogen-bonded peaks gradually decrease and shift to higher wavenumbers until they fully disappear, while the free carbonyl peak increases. When the material is cooled, the free and hydrogen-bonded amine and carbonyl peaks are restored, indicating the thermoreversible breaking and formation of the hydrogen-bonding interactions.

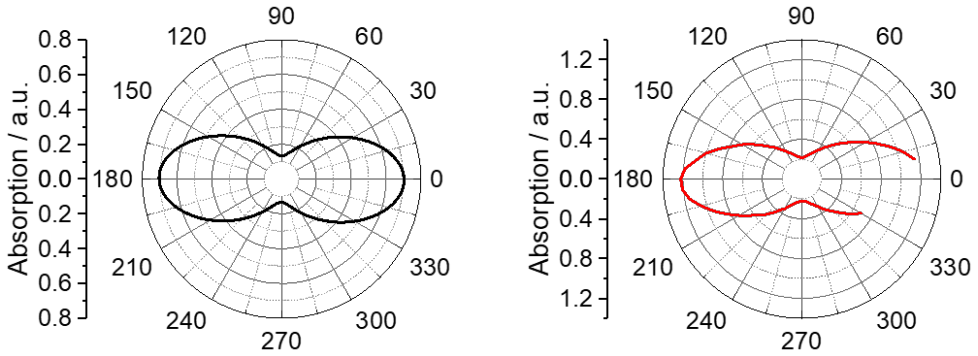

Figure S10. Azimuthal plot of polarized transmission FT-IR spectroscopy with absorption frequency $\tilde{\nu}$ = 1605 cm^{-1} corresponding to the C=C stretching vibrations of the benzene rings (left). Azimuthal plot of UV-vis absorption measurements with λ = 365 nm characteristic for the azobenzene moiety (right). The order parameter $S = (D-1)/(D+2)$ is calculated using the dichroic ratio $D = A_{\parallel}/A_{\perp}$.

FT-IR ($\tilde{\nu}$ = 1605 cm^{-1}): $D = 0.652 / 0.123 = 5.301$

$S = 4.301 / 7.301 = 0.589$

UV-vis (λ = 365 nm): $D = 1.248 / 0.223 = 5.596$

$S = 4.596 / 7.596 = 0.605$

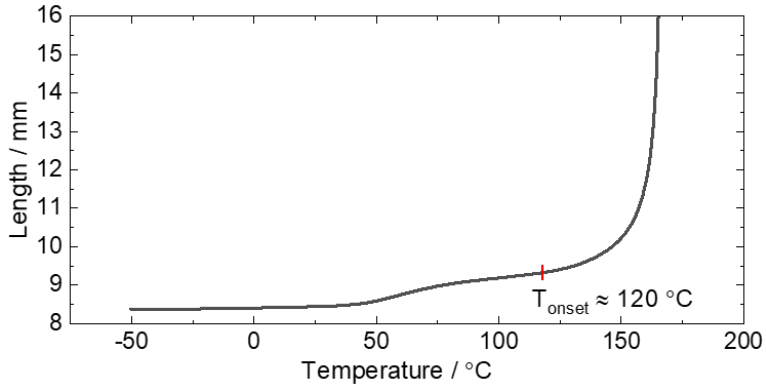

Figure S11. Constant force (iso-stress) experiment of compression-molded PTU with σ = 10 kPa. The small enlargement around the T_i is attributed to a change in material properties, whereas the distinct increase in length arises from the plastic flow.

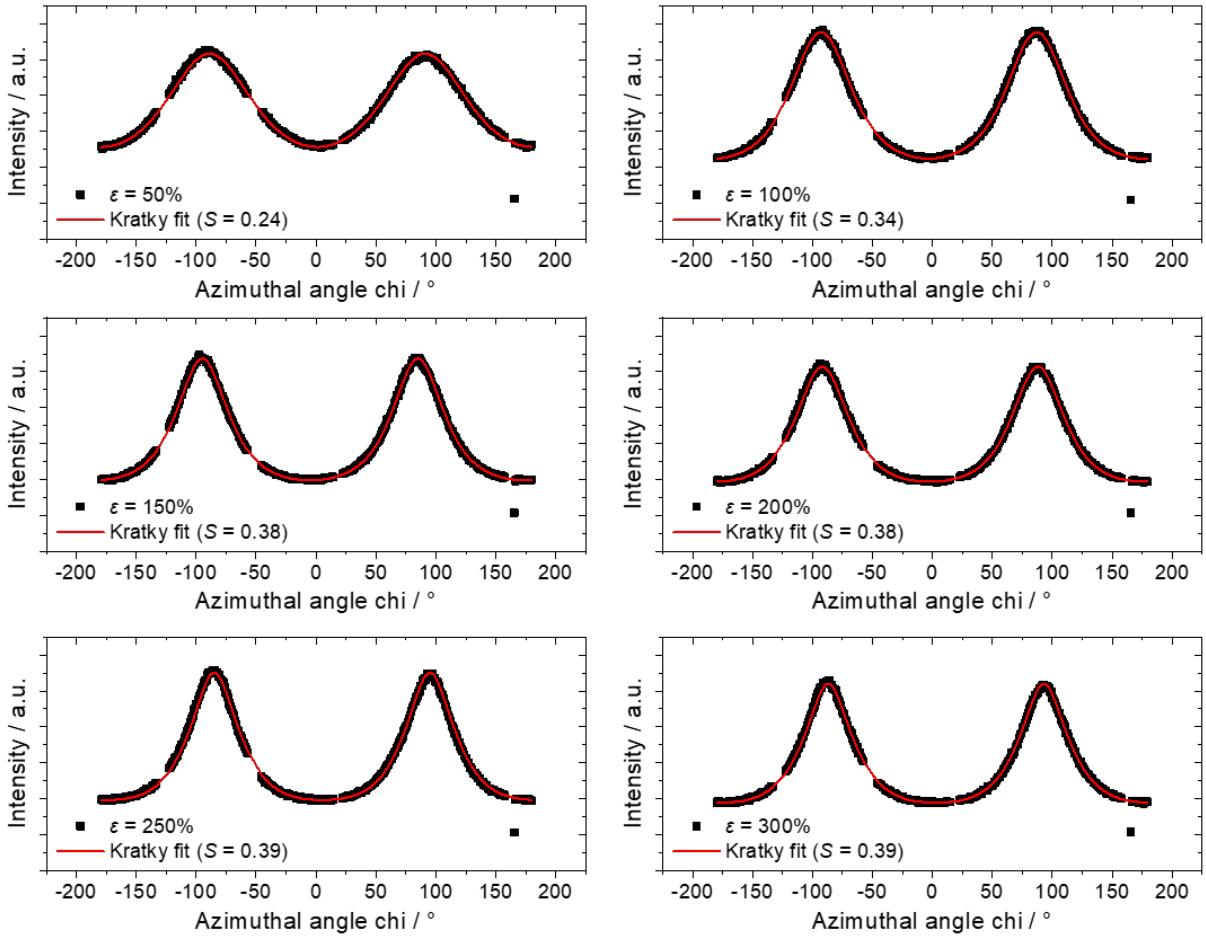

Figure S12. Azimuthal profiles of the 2D WAXS patterns at q_a = 14.3–14.6 nm^{-1} for the mechanically programmed PTUs with different programming strains (ε = 50–300%). The order parameter was obtained by fitting a Kratky function over the azimuthal angle with a custom-made script.

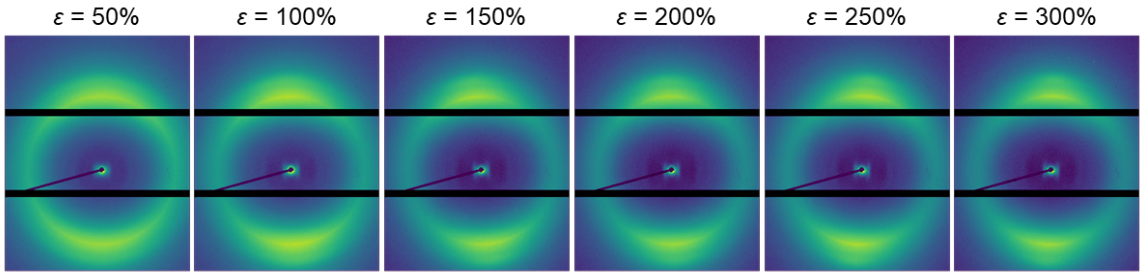

Figure S13. 2D WAXS diffractograms of mechanically programmed PTUs with different programming strains (ε = 50–300%). The molecular orientation of the materials is horizontal.

Table S1. Overview of the mechanical programming results for the preparation of actuators with different strains (ε = 50–300%) and the corresponding actuation strain and order parameter.

	Programming			**Actuation**	
Sample	ε_0 [a]	ε_f [b]	$\varepsilon_f - \varepsilon_0$	ε_a [c]	***S***
1	50%	70%	20%	14%	0.24
2	100%	135%	35%	22%	0.34
3	150%	171%	21%	24%	0.38
4	200%	219%	19%	27%	0.38
5	250%	246%	-4%	26%	0.39
6	300%	281%	-19%	26%	0.39

[a] Set programming strain; [b] Strain after programming; [c] Actuation strain.

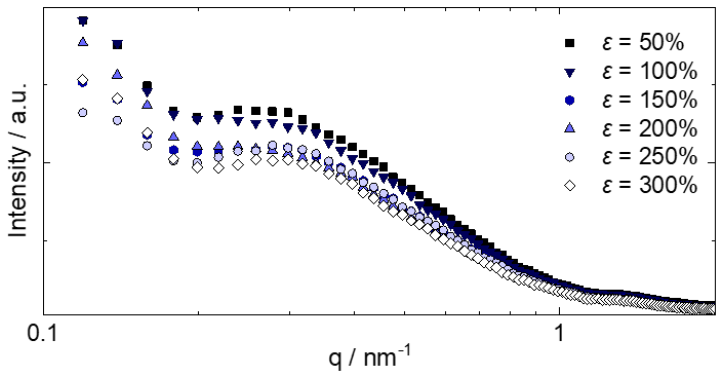

Figure S14. 1D MAXS diffractograms of the PTUs with different programming strains (ε = 50–300%).

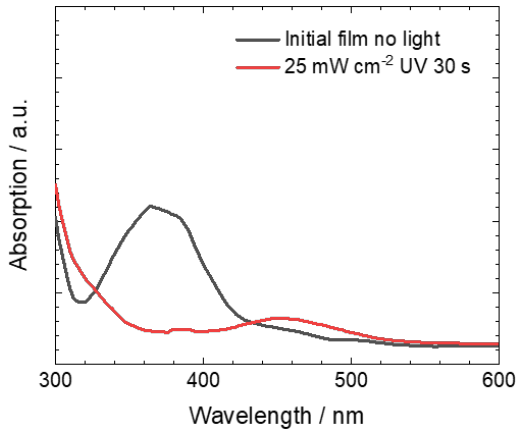

Figure S15. UV-vis absorption spectra of a thin (1.5 µm) supramolecular LCE film containing 3 mol% azobenzene before (grey line) and after (red line) illumination with UV light (365 nm, 25 mW cm^{-2} for 30 s).

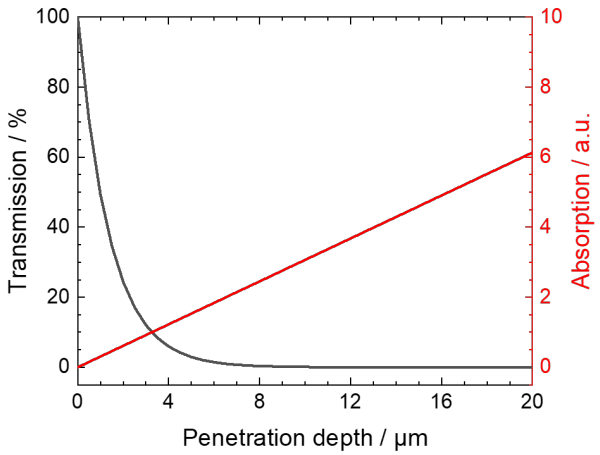

Figure S16. Transmission and absorption as a function of the penetration depth of the azobenzene containing PTU as obtained by theoretical calculation. From the Lambert-Beer law, the absorption coefficient (0.31 μm^{-1}) was determined based on the absorption at λ =365 nm of a 1.5 µm thick sample (3 wt% of **3**), which is extrapolated as a function of the penetration depth.

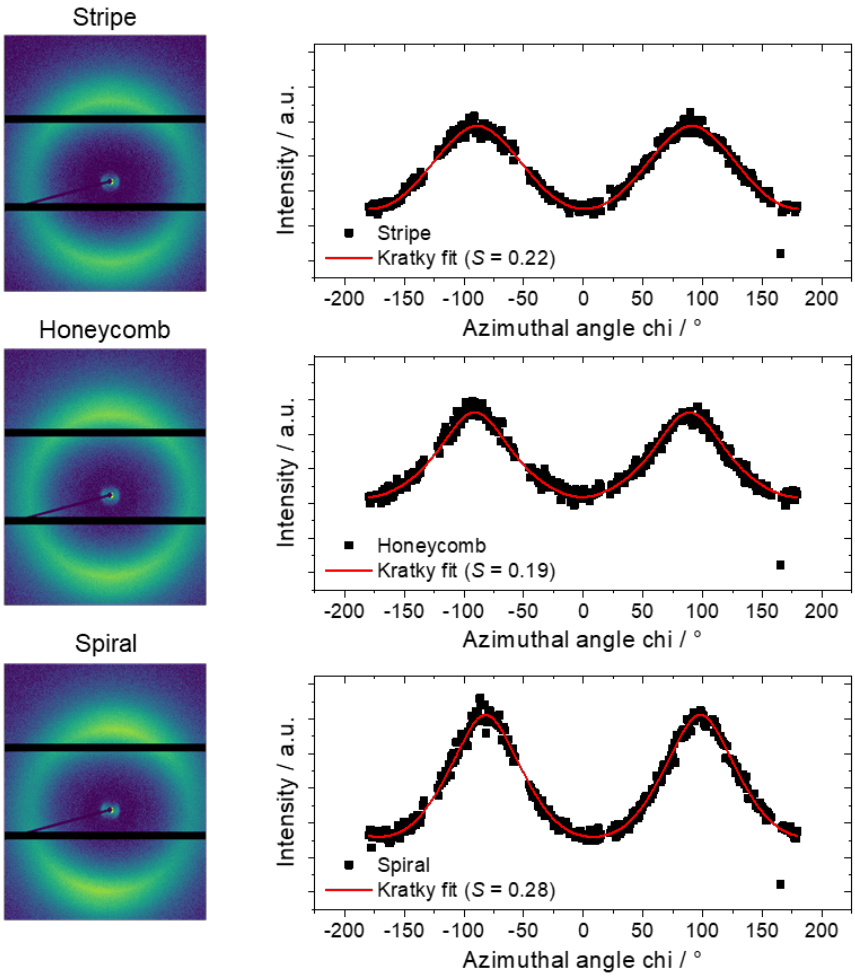

Figure S17. 2D WAXS patterns (left) and corresponding azimuthal profiles (right) of the printed stripe, auxetic honeycomb, and spiral director structure obtained with DIW. The order parameter was obtained by fitting a Kratky function over the azimuthal angle by a custom-made script at q_a = 14.3–14.6 nm^{-1}.

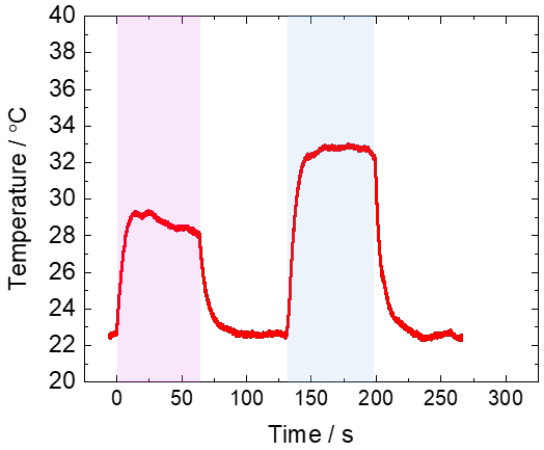

Figure S18. Temperature profile of the photoactuation without weight in air of the printed actuator stripes. Upon UV light illumination (25 mW cm^{-2}, violet region), the sample reaches temperatures just below 30 °C, whereas with blue light illumination (35 mW cm^{-2}, blue region), a temperature of 33 °C is reached.

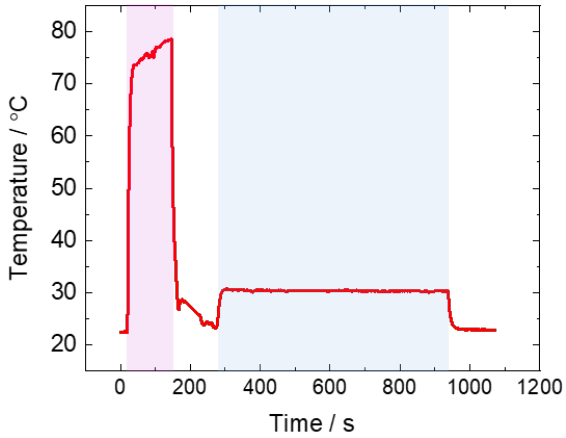

Figure S19. Temperature profile of the photoactuation with weight in air of the printed actuator stripes. Upon UV light illumination (220 mW cm^{-2}, violet region), the sample reaches temperatures of just below 80 °C, whereas with blue light illumination (15 mW cm^{-2}, blue region), a temperature of 30 °C is reached.

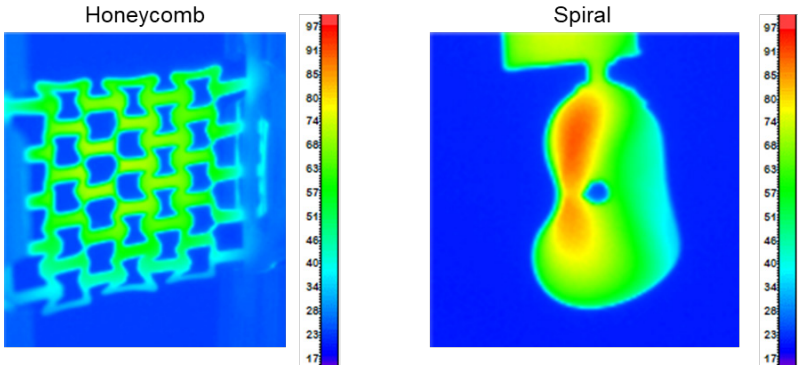

Figure S20. Thermography images of the complex structures. During photoactuation, temperatures of around 78 °C are reached for the auxetic honeycomb, while for the spiral director structure temperatures up to 90 °C are observed. It is apparent that during light actuation, the samples are inhomogeneously heated.

Calculating the activation energy (E_a) from the Arrhenius equation

Thermal stress-relaxation experiments were performed with temperatures from 100 to 150 °C with a constant strain ε = 100%. From this data, the relaxation constant τ^* can be obtained, which is defined as $\sigma/\sigma_0 = e^{-1}$ (i.e., stress relaxation modulus σ_0 reaches 37% of its initial value). Accordingly, the characteristic relaxation times τ^* are plotted versus 1000 T^{-1} and fitted to the Arrhenius equation:

$$\tau^*(T) = \tau_0 e^{E_a/RT}$$

In this equation, T is the temperature (K), R is the molar gas constant (8.314 J K^{-1} mol^{-1}), τ_0 is the characteristic relaxation time at 1000 T^{-1} = 0 (y-intercept), and E_a is the activation energy (kJ mol^{-1}). The activation energy can be determined by transforming the Arrhenius equation to the following:

$$\ln \tau^*(T) = ln\, \tau_0 + E_a/RT$$

From the linear relationship in Figure 2b, the activation energy can be calculated as follows:

$$\ln \tau^*(T) = -42.3 + 19.5 * 1000/T$$
$$E_a/R = 19.5 \text{ (slope)}$$
$$E_a = 19.5 * R = 162 \text{ kJ mol}^{-1}$$

Hence, the activation energy E_a is derived from the Arrhenius equation: 162 kJ mol^{-1}.

Calculating the specific work capacity from the photoactuation with load

The weight-specific work capacity can be calculated from the following equations:

$$\text{Specific work capacity} = W/m_{\text{sample}}$$
$$W = F * s$$
$$F = m_{\text{load}} * g$$

In these equations, W is the amount of work (J) performed during photoactuation, m_{sample} is the mass (kg) of the sample, F is the applied force (N), s is the displacement (m), m_{load} is the mass (kg) of the attached weight, and g is the gravitational acceleration (m s^{-1}). The specific work capacity of the photoactuation (14.4% contraction: s = 1.96 mm) of the printed actuator (m_{sample} = 8 mg) with load (m_{load} = 1 g) in air using high-intensity UV (220 mW cm^{-2}) can be calculated as follows:

$$F = 0.001\ \text{kg} * 9.81\ \text{m s}^{-1} = 0.01\ \text{N}$$
$$W = 0.01\ \text{N} * (1.96 * 10^{-3})\ \text{m} = 1.92 * 10^{-5}\ \text{J}$$
$$\text{Specific work capacity} = (1.96 * 10^{-5}\ \text{J})/(8 * 10^{-6}\ \text{kg}) = 2.4\ \text{J kg}^{-1}$$

The specific work capacity of the photoactuation (4.5% contraction: s = 0.57 mm) of the printed actuator (m_{sample} = 8 mg) with load (m_{load} = 0.75 gram) in water using high-intensity UV (220 mW cm^{-2}) can be calculated in the same manner (note that the apparent weight of the load is corrected for the underwater experiment):

$$F = 0.00075\ \text{kg} * 9.81\ \text{m s}^{-1} = 0.007\ \text{N}$$
$$W = 0.007\ \text{N} * (0.57 * 10^{-3})\ \text{m} = 0.42 * 10^{-5}\ \text{J}$$
$$\text{Specific work capacity} = (0.42 * 10^{-5}\ \text{J})/(8 * 10^{-6}\ \text{kg}) = 0.5\ \text{J kg}^{-1}$$

Supporting video captions

Video S1. Photoactuation of the programmed PTU actuator in air. Playback rate: 4×.

Video S2. Underwater photoactuation of the programmed PTU actuator. Playback rate: 4×.

Video S3. Photoactuation of the printed PTU actuator with load in air. Playback rate: 16×.

Video S4. Photoactuation of the printed re-entrant honeycomb. Playback rate: 16×.

Video S5. Photoactuation of the printed spiral director structure. Playback rate: 16×.